Embedded Sensors in Sandwich Composite Materials with Cork Agglomerate Core

Joana Osório Gomes Rosado de Sousa
joana.d.sousa@tecnico.ulisboa.pt

Instituto Superior Técnico, Universidade de Lisboa, Portugal

July 2019

Abstract

This study intends to assess how embedded sensors can change the mechanical properties of a sandwich composite material with cork agglomerate core and fibreglass and epoxy resin skins. The behaviour of the material was analysed during tensile, flexural and creep tests, in three different situations: without sensors, with surface sensors and with embedded sensors. The sensors tested were strain gages and fiber Bragg grating. The manufacturing process used to produce the composite specimens was the hand lay-up process, which proved to allow good measurements from the embedded sensors. Collected data analysis showed that embedded sensors affected the flexural resistance and failure modes. In the creep test, the specimens were sensible to the highest temperature, and all the data collected by the sensors translated this difference. The stiffness analysis did not allow to draw conclusions due to the small number of specimens, but the fact that some specimens with embedded sensor showed no significant changes in stiffness, compared with specimens without sensors and surface sensors, reinforces the need to continue with studies in this area that can allow to validate and generalize results. This study followed the objectives proposed, increasing knowledge regarding this subject. The conclusions open a way to future studies that can test a larger number of specimens, develop numerical simulations to compare results and perform other tests that can allow characterizing the effects of embedded sensors in the behaviour of this materials.

Keywords: Embedded sensors, Strain Gage, Fiber Bragg Grating, Structural Health Monitoring, Sandwich composite

1. Introduction

Many industries, such as the aerospace industry, would not have achieved their high performance if composite materials had not been used [6]. Among the various types of composites, sandwich composites are widely used in various applications such as satellites, aircraft and energy systems [15]. The sandwich composite typically consists of two external skins, separated by a thicker inner core. In these structures, the flexural rigidity and strength are substantially increased compared to a laminate composite [9].

There are several types of cores used in sandwich composites. Since cork is a material that has high shear strength, low specific weight, high damage tolerance to impact loads, resistant to friction and both good thermal and acoustic insulation capacity, it is a good candidate for the core [3].

Despite having advantages over other types of composites, sandwich structures have complex failure modes, which may cause a significant decrease in the mechanical properties of the material. Consequently, it is essential to continuously monitor these structures to ensure their structural integrity [15] [2].

The process of implementing a strategy for detection and characterization of damage for engineering structures is known as Structural Health Monitoring (SHM). This process monitors a structure over time, using a series of sensors [7].

The layered configuration of a composite makes it difficult to predict their structural behavior using only surface sensors, since they cannot effectively monitor the internal damage. In order to solve this problem, the embedded sensors appear as the best alternative, reaching areas that are difficult to reach from the outside. The sensors embedded can, however, interfere with the material properties [7].

In order to conclude about the influence of embedded sensors on the mechanical properties of a sandwich composite with cork agglomerate core and fiberglass and epoxy skins, with a view to its application in future engineering projects, an exploratory study was carried out in which the tensile, flexural and creep behaviour of this material was analyzed in three different situations: without

sensors, with surface and with embedded sensors. The sensors used were strain gages and fiber Bragg grating [13] [8].

2. Background

2.1. Cork Agglomerate

The properties of primary interest for the core materials are: low density, high shear modulus, high shear strength, high stiffness perpendicular to the faces, and good thermal and acoustic insulation characteristics. Cork agglomerates have shown some remarkable properties when used as a core of sandwich composites, namely high damage tolerance caused by impact loads, good thermal and acoustic insulation capacity, as mentioned above, and excellent damping characteristics for the suppression of vibrations [3].

2.2. Visual Image Correlation (VIC)

The VIC system is based on the analysis of consecutive images, obtained before and after deformation of an object, through a correlation algorithm. The initial image is divided into several blocks or subsets that are searched in the next image. Each block corresponds to a set of pixels and the algorithm allows to determine its new position, looking for the values of intensities of these pixels, and calculates the motion that the block performed from one configuration to another, allowing to calculate displacements and strains [14].

To use the VIC system, the surface of the material needs to be conveniently prepared by applying a speckled pattern. This pattern can be created by painting the sample with a white spray and then placing spots with a black colour spray, each with a similar diameter. The pattern cannot be repetitive, otherwise there might be more than one match for a specific block, which causes a phenomenon of de-correlation [16] [14].

2.3. Strain Gages

The strain gage is a resistive sensor used to measure strains. The relationship between the applied strain ε ($\varepsilon = \Delta L/L_0$) and the relative change of the resistance of the strain gage is proportional and can be described by the following equation:

$$\frac{\Delta R}{R} = GF \times \varepsilon \tag{1}$$

where GF, known as the gage factor, is a characteristic of the strain gage and can be obtained experimentally [5] [4].

The relative changes of resistence in the strain gage are very small, usually around 10^3 Ω/Ω. Therefore, the sensor must be integrated in a system that allows this changes of resistence to be measured with great accuracy. This system generally consists of a Wheatstone bridge circuit [4].

2.4. Fiber Bragg Grating (FBG)

A FBG is a periodic and permanent modification of the core refractive index value of an optical fiber along its longitudinal direction. When the FBG is illuminated by a broadband light source, the periodic grating acts as a filter, reflecting a portion of the initial spectrum. The total intensity of the wave is determined by the overlap of all the individual reflected components, presenting a maximum of amplitude when these are in phase. This maximum amplitude value is called the Bragg wavelength, λ_B, and is given by the Bragg condition:

$$\lambda_B = 2n_{ef}\Lambda \tag{2}$$

where n_{ef} is the effective refractive index of the fiber core and Λ is the grating period [11].

3. Implementation

3.1. Materials

The material produced and tested consisted of a sandwich composite with cork agglomerate core and fiberglass and epoxy resin skins. The cork agglomerate used was the NL20, provided by ACC®, with a thickness of 10 mm. The glass fiber used was the 205 g/mm^2 fiber and the resin was the Resoltech 1050 Infusion Epoxy with the hardener 1059S, both provided by Castro Composites®.

The composite was produced using the hand lay-up method.

3.2. Sensors and Acquisition Systems

The strain gages selected were the 1-LY16-6/350 (HBM®). For the acquisition system, it was used the NI cDAQ-9178 equipment with the Wheatstone bridge interface module NI-9237, both produced by National Instruments®. The NI cDAQ-9178 communicates with a computer running LabVIEW software.

The fiber Bragg grating sensors used were the K-FS62 - Miniature Polyimide Strain Sensor(HBM®). The data acquisition system consisted of the interrogator sm125-200 (uMicron®). The ENLIGHT software is responsible for the user interface.

3.3. Testing machine and validation systems

The test machine used was the Instron® 5566 with a load cell of 500 N for flexural tests and 10 kN for tensile tests. This machine was linked to the Bluehill's software.

To compare/validate the results, it was used the digital image correlation system by Correlated Solutions® VIC-2D, consisting of VIC-Snap and VIC-2D, and the clip gage. The clip gage used was the 2630-106 with a gauge length of 25 mm and a measuring range from $+12.5$ to -2.5 mm.

3.4. Tensile tests

For the tensile test configuration, it was followed the method described by Ramos [12], which consists of using metallic sheets at each end of the specimen and creating a hole in the centre. Each hole is crossed by a pin and then attached to the moorings of the machine. To glue the metallic sheets it was used the same epoxy resin as in the composite production and the Akepox 2030 resin. None of them worked, because all of the sheets unstuck from the specimen. However, it was possible to get a notion on the location of the elastic zone, allowing the continuation of the tests with the sensors.

Table 1: Tensile test prototypes.

Batch	Specimen	Sensor position
TA	TA1	No sensor
	TA2	No sensor
TB	TB1	No sensor
	TB2	No sensor
TC	TC1	No sensor
	TC2	No sensor
	TC3	No sensor
	TC4	No sensor
	TC5	No sensor
	TC6	No sensor
	TC7	No sensor
TD	TD1	No sensor
	TD2	No sensor
	TD3	No sensor
	TD/SG1/S	1 Surface
	TD/SG2/E	1 Embedded
	TD/FBG1/E	1 Embeded
TE	TE1	No sensor
	TE2	No sensor
	TE3	No sensor
	TE/SG1/S	1 Surface
	TE/SG2/E	1 Embedded

The specimen's geometry was chosen based on the values used by Ramos [12]: width of 20 mm, length of 200 mm and total thickness of 10 mm. Regarding the speed of the cross of the machine, the value of 3 mm/min was selected.

Table 1 shows the prototypes that were produced and tested. All instrumented specimens have a quarter bridge configuration. The calculated parameters are described next.

3.4.1 Poisson's ratio calculation

The Poisson's ratio value was calculated according to the standard *E 132 - 04 Standard Test Method for Poisson's Ratio at Room Temperature*. The standard proposes the use of strain gages for this calculation, however, the same approach was followed using the VIC-2D software instead of the sensors. Two perpendicular lines were drawn in the center of the specimen, in the VIC-2D analysis, each with a length of 20 mm, using the *Inspect Extensometer* command. This command allows the obtention of engineering strains.

Following the standard, two graphs were drawn: the longitudinal strain (ε_L) vs load (P) and transversal strain (ε_T) vs load (P). Using a linear regression, the slopes of the two lines were calculated and by applying equation 3, the Poisson's ratio for each specimen was obtained.

$$\mu = \frac{d\varepsilon_T/P}{d\varepsilon_L/P} \tag{3}$$

3.4.2 Young's modulus

For Young's modulus (E) calculations, the standard *E 111-97 Standard Test Method for Young's Modulus, Tangent Modulus, and Chord Modulus* was followed.

The range of load values chosen for these calculations was from 150N to 500N, which guarantees that the material stays within the elastic regime. The instrument used to compare the values of E, obtained from the surface sensors, was the clip gage. For the embedded sensors, it was used the VIC-2D for comparison.

3.4.3 Area analysis

In this analysis, the TD and TE batches were used, painted with the pattern required for the VIC-2D analysis. The mean Young's modulus corresponding to three different areas were obtained using the VIC-2D *Inspect Rectangle* command. This command allows the obtention of the Lagrange strains. Three areas were chosen (Figure 1): area of the sensor (A1), area above the sensor (A2) and a global area (A3).

One of the objectives of this analysis is to verify if the VIC system is sensitive to the presence of the strain gage, that is, if the influence of the incorporation of the sensor in the stiffness is detected, when compared with specimens without sensors.

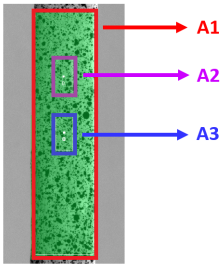

Figure 1: Area analysis.

3.5. Flexural tests

In flexural tests, two versions of the standard ASTM C393: *C393/00 Standard Test Method for Flexural Properties of Sandwich Constructions* and *C393 / C393M Standard Test Method for Core Shear Properties of Sandwich Constructions by Beam Flexure* were followed. The four-point bending and three-point loading configuration was chosen. Regarding the speed of the cross of the machine, the value of 6 mm/min was selected, as suggested by the standards.

By following the constraints imposed by C393/C393M for a four-point configuration, the following dimensions were chosen for the specimens: 50 mm width, 10 mm core thickness, 11 mm total thickness and a distance between the lower supports of 270 mm.

The following table shows the prototypes that were produced and tested.

Table 2: Flexural test prototypes.

Batch	Specimen	Sensor Position	Bridge Configuration
FA	FA1	No sensor	-
	FA2	No sensor	-
	FA3	No sensor	-
FB	FB1	No sensor	-
	FB2	No sensor	-
	FB3	No sensor	-
	FB/SG1/S	Surface	Half
	FB/SG2/S	Surface	Half
FC	FC1	No sensor	-
	FC2	No sensor	-
	FC/SG1/S	Surface	Quarter
	FC/SG2/S	Surface	Half
	FC/SG3/S	Surface	Full
	FC/SG1/E	Embedded	Quarter
	FC/SG2/E	Embedded	Half
	FC/SG3/E	Embedded	Full
FD	FD/FBG1/E	Embedded	Quarter
	FD/SG1/E	Embedded	Quarter

The calculated parameters are described in the following section.

3.5.1 Maximum failure load

To be able to carry out repeatability tests on the instrumented specimens, up to a maximum load value within the region of the elastic regime, destructive flexural tests were carried out using batches FA and FB in order to obtain this parameter.

3.5.2 Calculation of neutral axis and flexural Young's Modulus

Mujika et al [10] describes a method for determining the neutral axis position ($\sqrt{\lambda}$). Firstly, the specimen is placed on the test machine in a four-point bending configuration with the strain gage on the compressive side. The load-strain curve is recorded. Then, the same specimen is put on the test machine with the strain gage on the tensile side and the load *vs* strain curve is obtained. Considering m_T as the slope of the load *vs* strain curve on the tensile side and m_C as the slope of the load *vs* strain curve on the compressive side, the position of the neutral axis is calculated, using the following equation:

$$\frac{m_T}{m_C} = \frac{P/\varepsilon_T}{P/\varepsilon} = \frac{h_C}{h_T} = \sqrt{\lambda}. \tag{4}$$

The above equation also shows the position of the neutral axis, expressed in terms of the ratio between the thickness of the test specimen in compression (h_C) and the thickness of the specimen in tensile (h_T).

Having the value of $\sqrt{\lambda}$, the flexural Young's modulus, E_F, can be calculated using the following equation:

$$E_F = \frac{4}{(1+\lambda)^2}\frac{3m_T L}{8bh^2}(1+\sqrt{\lambda}) \tag{5}$$

where L is the distance between the points at which the specimen is supported during the test, b the width of the specimen and h its thickness.

Each test ended when the load reached approximately 40 % of the maximum load obtained in section 3.5.1, ensuring that the specimen remained in the elastic region.

For the embedded sensors, it was not possible to directly apply the previous equation to obtain the value of E_F, since it was deduced considering the strain measurement at the surface of the specimen. To correct this situation, knowing the strain value at the interface, ε_2, read by the sensor, the expected strain value at the surface ε_1 can be calculated considering that the specimen is in pure bending [1]:

$$\varepsilon_1 = \frac{h_C}{h_T - t_F}\varepsilon_2. \tag{6}$$

3.5.3 Effect on resistance

After the repeatability tests, flexural tests were performed on the FC batch specimens but this time until failure, in order to conclude how the introduction of surface and embedded strain gages could influence the strength of the specimen.

3.6. Creep tests

There are no creep tests standards for sandwich composites. As such, the temperature values were based on the standard *ASTM D2990-01: Standard Test Methods for Tensile, Compressive, and Flexural Creep and Creep Rupture of Plastics*. The creep tests were performed using the flexural test configuration and specimens dimensions, with distributed loads of 12N.

Each test was performed in the Memmert incubator, during five hours. All specimens were tested at two temperatures: 23°C and 70°C. Table 3 shows the prototypes that were produced. All strain gages are in a quarter bridge configuration.

Table 3: Creep test prototypes.

Batch	**Specimen**	**Sensor Position**
C1	C1/FBG1	1 Embedded
	C1/SG1	1 Embedded
C2	C2/SG1	1 Embedded
	C2/SG2	1 Embedded
C3	C3/SG1	1 Embedded

The calculated parameters are described next.

3.6.1 Measure of ΔL_{Final}

After each creep test, the value of ΔL_{Final} (Figure 2) was measured for each specimen using a millimetre sheet. The objective was to verify the influence of a high temperature and the distributed load on the behaviour of the specimen with the embedded sensor.

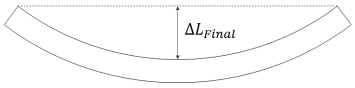

Figure 2: ΔL_{Final} value.

3.6.2 Creep test graphs

After each creep test, the curve strain-time was obtained, in order to understand the behaviour of the sensor with the increase in temperature and the differences observed between the two types of sensors.

4. Results

4.1. Tensile tests

Table 4 shows the values of the Poisson's ratio calculated, the mean value ($\overline{\nu}$) and the standard deviation (SD). There were small variations between the ν values of specimens of the same batch and specimens of different batches. This variability observed in specimens from the same batch may be due to: cork agglomerate's heterogeneity; variation of resin distribution along the specimen as a consequence of the hand lay-up process; the lower pressure and temperature action on the specimens positioned in the peripheral zone of the press.

Table 4: Values of Poisson's ratio (ν) for each specimen, mean value ($\overline{\nu}$) and standard deviation (SD).

Batch	**Specimen**	ν	$\overline{\nu}$	SD
TA	TA1	0,18		
	TA2	0,19	**0,18**	**0,01**
TB	TB1	0,18		
	TB2	0,15	**0,17**	**0,02**
TC	TC1	0,17		
	TC2	0,18		
	TC3	0,18		
	TC4	0,18		
	TC5	0,18		
	TC6	0,19		
	TC7	0,16	**0,18**	**0,01**
TD	TD1	0,18		
	TD2	0,18		
	TD3	0,16	**0,17**	**0,01**
TE	TE1	0,18	-	-
			0,18	**0,01**

The variability between specimens of different batches is, in addition to the causes mentioned above, due to the fact that they were produced at different time intervals. This means they were placed in the press and in the furnace at different times, and while maintaining the pressure of 1 *bar* and the temperature of 60°C, it was not possible to ensure the absence of fluctuations in these parameters, which occur at different manufacturing times.

These variations may also be associated with inaccuracies in the VIC system: difference sizes between black spots, with some of them too small, which may have caused aliasing, even though a low-pass filter was used; inadequate placement of light, reducing the detail of the points in the image; the fact that the light is too hot and can change the refractive index of the air in the optical path, which can also lead to uncertainties in the final results obtained; an incorrect alignment using the *Inspect Extensometer* command.

Figure 3 (see last page) shows the tensile test results regarding the Young's Modulus (E) calculation. The tension-strain curves are presented for the specimens without sensors, with surface sensors and embedded sensors of the batches TD and TE. In the specimens without sensors, the values of the strains were obtained using only the VIC system. In the specimens with surface strain gages, the values were obtained using the sensor and clip gage and, in the specimens with embedded sensors, using the

sensor and the VIC system.

For each tensile-strain curve obtained, the value of E was calculated using a linear regression model. This model can be applied since all graphs showed a linear relation and the Pearson correlation coefficients (R^2) were close to 1.

Considering all specimens without sensors of the batches TD and TE, it can be seen that regarding TD, the average value of E of the three tests is $856,5\ MPa$, with a standard deviation of 19.7. For the batch TE, only the results of two specimens are presented, since the third specimen had its metallic sheets unstuck at the beginning of the test. The TE2 test specimen has a lower load range since the metallic sheets unstuck before the specimen reached a load of 500 N.

Comparing the specimens without sensors of the two batches, it is possible to verify that the two values of E of the batch TE are superior to the three values of E of the batch TD, according to the data obtained using VIC, which suggests that the batch TE is the most rigid. The differences in stiffness between the two batches and within each batch may have occurred due to the causes associated with the variability between specimens and possible errors associated with the use of VIC, mentioned before.

Table 5 shows the relative errors defined as the ratio between the difference of the values of E obtained with the sensor and the systems VIC/clip gage, and the value of E obtained with the sensors.

Table 5: Relative errors.

Specimen	**System**	**Error Test 1**	**Error Test 2**	**Error Test 3**
TD/SG1/S	*C.G.*	21 %	-	-
TD/SG1/E	*VIC*	1 %	2 %	3 %
TD/FGB/E	*VIC*	10 %	20 %	-
TE/SG1/S	*C.G.*	32 %	27 %	23 %
TE/SG1/E	*VIC*	2 %	1 %	1 %

Considering the specimens with surface strain gages of both batches, it can be seen that in the specimen TD/SG1/S, only one test was performed, since the metallic sheets unstuck in that test with a load of 451 N. The relative errors between the values of E obtained with the strain gage and the clip gage were 21 % for the TD/SG1/S sample and around 28 % for the TE/SG1/S. This variation may have been caused by incorrect placement of the clip gage on the specimen, low accuracy of the clip gage to be used in a specimen with a small thickness or poor calibration of the instrument.

Considering the specimens with embedded strain gages in both batches, one of the conclusions can be derived from the embedded sensors reading the strain values, which means that the method used for their incorporation worked. The curves corresponding to the 2° and 3° tests have an offset of 0.0004 (mm/mm), along the x-axis, to help in the visualization.

The fiber Bragg grating sensor embedded in the specimen TD/FBG1/E failed during the third test. In the first two tests, it was possible to register values up to 300 N. This problem may be associated with a manufacturing defect in the Bragg sensor itself or an error introduced during its incorporation.

Considering the embedded strain gages of both batches, it is observed that the value of E obtained using VIC is close to the one given by these sensors. Table 5 quantifies this small difference, with an average relative error of 2% for TD/SG1/E and 1% for TE/SG1/E. The fact that the differences between the strain values read on the surface (VIC-2D) and the values read at the interface (strain gages) is small, suggests that the embedded process was well executed, which means that the incorporation of the strain gage in the interface did not interfere in the adhesion between the fiber and the cork agglomerate.

With respect to the comparison between specimens without sensor and specimens with embedded sensors, there was an increase in stiffness with the incorporation of the embedded strain gage in the batch TD, while in TE the value of the TE1 specimen was close to the values of the three tests of the specimen TG/SG1/E. This discrepancy between the batches does not allow a conclusion about the effect of embedded sensors in the stiffness properties of the material.

4.1.1 Area analysis

It was verified that there was an increase of the percentual difference between the areas with the incorporation of the sensors. It is also observed that there is mainly an increase in the stiffness in the sensor region (A3) compared to the global region (A1) and the region above the sensor (A2). This difference in the behaviour between instrumented and non-instrumented specimens, demonstrated by VIC, shows that the material is affected in some way, although not very significantly, by the presence of the sensor. In addition, it is possible to conclude that the VIC system, despite reading surface strains, is sensitive to the presence of embedded sensors and that, as such, it can be used as a useful tool in the study of embedded sensors in materials.

4.2. Flexural tests

4.2.1 Calculation of neutral axis and flexural Young's Modulus

Table 6 shows the values of the position of the neutral axis for each repeatibility test ($\sqrt{\lambda}_1$,$\sqrt{\lambda}_2$,$\sqrt{\lambda}_3$)

of specimens with surface sensors and the mean value ($\overline{\sqrt{\lambda}}$).

Table 6: Values of $\sqrt{\lambda}$ obtained for each repeatability test of specimens FB and FC and mean value ($\overline{\sqrt{\lambda}}$).

Specimen	$\sqrt{\lambda}_1$	$\sqrt{\lambda}_2$	$\sqrt{\lambda}_3$	$\overline{\sqrt{\lambda}}$
FB/SG1/S	1,0	1,0	1,0	1,0
FB/SG2/S	0,99	0,99	0.99	0,99
FC/SG1/S	0,97	0,98	0.98	0,97
FC/SG2/S	0,95	0,95	0.95	0,95
FC/SG3/S	1,0	1,0	1,0	1,0
				0,98

The mean value obtained suggests that the neutral axis of the material, although quite close to the center, results in average in a greater section of the specimen that is in the tensile side ($h_C = 0.98h_T$).

Table 7 shows the values of E_F calculated using the equations presented by Mujika et al. [10], for the three repeatability tests of batches FB, FC and FD.

Table 7: Values of E_F and mean value $\overline{E_F}$ for specimens FB, FC and FD.

Specimen	E_{F_1}	E_{F_2}	E_{F_3}	$\overline{E_F}$
FB/SG1/S	1710,7	1717,0	1713,1	1713,6
FB/SG2/S	1639,5	1638,2	1638,0	1638,6
FC/SG1/S	1921,5	1923,9	1920,5	1922,0
FC/SG2/S	2223,5	2214,2	2221,9	2219,9
FC/SG3/S	1908,7	1908,0	1908,5	1908,4
FC/SG1/E	1859,5	1856,5	1886,0	1867,3
FC/SG2/E	1996,2	1978,1	2002,9	1992,4
FC/SG3/E	2189,9	2197,6	2199,5	2195,7
FD/FBG1/E	2659,3	2655,7	2653,4	2656,1
FD/SG1/E	2746,5	2764,9	2772,2	2761,2

Table 8: Percentage difference (DP) between specimens FB, FC and FD.

Specimen 1	**Specimen 2**	PD (%)
FB/SG1/S	FB/SG2/S	4
FC/SG1/S	FB/SG2/S	13
FC/SG1/S	FC/SG3/S	1
FC/SG2/S	FC/SG3/E	14
FC/SG1/E	FC/SG2/E	6
FC/SG1/E	FC/SG3/E	15
FC/SG2/E	FC/SG3/E	9
FC/SG1/S	FC/SG1/E	3
FC/SG2/S	FC/SG2/E	10
FC/SG3/S	FC/SG3/E	13
FD/FBG1/E	FD/SG1/E	4

Observing the percentage difference between the values of $\overline{E_F}$, shown in table 8, is verified that there is variability between the specimens of the same batch and of different batches. The possible cause of these variabilities are described in section 4.1.

For the FC batch, regarding the specimens with surface sensors, it is possible to observe that the FC/SG2/S specimen has a higher percentage difference, in comparison with the specimens FC/SG1/S and FC/SG3/S. This difference might be associated with the fact that, because it is a half bridge configuration, the transverse sensor was not exactly perpendicular to the longitudinal sensor, affecting the measurement of the strains.

Regarding the percentage differences calculated between specimens of the FC batch with surface and embedded sensors, both with the same bridge configuration, it is verified that there is a greater deviation in half-bridge (FC/SG2/S and FC/SG2/E) and full bridge (FC/SG3/S and FC/SG3/E) configurations. Between the quarter-bridge configurations (FC/SG1/S and FC/SG1/E), the difference is lower, which indicates that the incorporation of the embedded strain gage and the strain gage on the surface had the same influence on the material stiffness.

In the FD batch, the percentage difference between the values of $\overline{E_F}$ of the specimen with the embedded strain gage and the specimen with the embedded fiber Bragg grating sensor is small. In this sample of two specimens, the incorporation of the two sensors had the same influence on the stiffness of the material.

All specimens with embedded sensors were not damaged during the tests and allowed to read the strain values, which means that the method chosen for their incorporation proved to be efficient. Regarding the fiber Bragg sensor, there was no error in the data provided by the sensors as it occurred in the tensile tests.

4.2.2 Effect on resistance

Table 9: Values of maximum tension (σ_{max}), mean value and standard deviation (SD).

Specimen	**Config.**	σ_{max} (MPa)	$\overline{\sigma_{max}}$ (MPa)	SD
FC1	No Sensor	7,5		
FC2	No Sensor	8,3	**7,9**	**0,4**
FC/SG1/S	Surface	8.0		
FC/SG2/S	Surface	7.7		
FC/SG3/S	Surface	8.2	**8,0**	**0,4**
FC/SG1/E	Embedded	6.2		
FC/SG2/E	Embedded	5.3		
FC/SG3/E	Embedded	4.8	**5,5**	**0,6**

Table 9 shows the maximum stress value (σ_{max}) obtained in the destructive tests of the specimens of the batch FC. In this analysis, the specimens were divided into three groups - without sensors, with surface sensors and embedded sensors - and the mean and standard deviation for each of them was calculated.

By analysing table 9, we verify that the value of the maximum stress of specimens without sensors (FC1 and FC2) was close to the value of specimens with surface sensors. The specimens with embedded sensors had a lower value of maximum stress, in comparison with the others. Also, there was a decrease in the strength with the increase of the number of strain gages embedded in the specimen.

Regarding the embedded sensores, the failure occured near the soldering of the sensores. The incorporation of the sensor, the weld and the wires may have introduce deffects in the adhesion between the core and the skins, weakening it, thus altering the strength properties of the composite material.

4.3. Creep tests

The creep tests were performed with the sensor in the tensile side, since the determination of the representative value of the position of the neutral line in the flexural tests allowed to realize that there is a greater section of the specimen that is at tensile, which means that this corresponds to the face that reads the largest strain values.

Table 10 shows the ΔL_F values, measured after each creep test.

Table 10: Values of ΔL_F.

Batch	**Specimen**	**N° Test**	**T (°C)**	ΔL_F (mm)
C1	C1/FBG1	Test 1	70	3
	C1/SG1	Test 1	70	3
		Test 2	70	0
		Test 3	23	1
C2	C2/SG1	Test 1	23	0
		Test 2	70	28
	C2/SG2	Test 1	70	6
C3	C3/SG1	Test 1	23	0.5
		Test 2	70	1.5

In the tests performed at 23°C, the value of ΔL_F recorded was lower, compared to the tests at 70°C, which presented a higher ΔL_F value. Although the exiguity of the sample does not allow to make conclusions, it was found that the material was sensitive to a higher temperature.

The specimens of the batch C1, with embedded fiber Bragg grating sensor (C1/FBG1) and embedded strain gage (C1/SG1), recorded the same final ΔL_F after the first test at 70°C, which means that, for this sample, the influence of the incorporation of the two types of sensors was similar in the deformability of the material. In the case of the specimen C1 /FBG1, it was possible to perform only one test. The attempt to perform a second test with this same sensor failed, due to the lack of signal. Although the fiber Bragg grating sensors used had a maximum operating temperature of 80°C and in this test a temperature of 70°C was used, the specimen was subjected to a test for 5 hours with a distributed load which may have caused damage to the sensor.

The two specimens of the batch C2 (C2/SG1 and C2/SG2) were more deformed than the others, after the tests at 70°C. This occurence may be associated with some deformation during the method of producing the agglomerate itself or during the manual process of hand lay-up.

Figure 4 presents the creep curves of all tests. The starting point of the graph corresponds to the moment after the placement of the distributed loads.

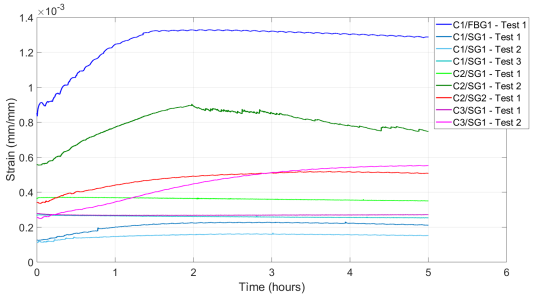

Figure 4: Creep curves.

By analyzing the creep curves, it was verified that the sample with Bragg sensor (C1/FBG1) presented higher values of strain during the test. This was the only sample in which a dummy was not associated for thermal compensation, so it is acceptable that the temperature variations occurred explain the final strain values.

Regarding the two specimens of the batch C2 that had a higher deformation, in the case of test specimen C2/SG1 - Test 2 at 70°C, it was obtained an anomalous curve with reduction of the strain between the second and the fifth hours, which corresponded to an erroneous sensor reading. In the case of specimen C2 / SG2 - Test 1, the deformation did not translate into any anomaly of the graph, possibly associated with the fact that the value of ΔL_F was much lower, which means that the sensor did not have an adequate reading of the state of the specimen.

5. Conclusions

In flexural tests, collected data analysis showed that embedded sensors affected the resistance and failure

modes. In creep tests, the specimens were sensible to the highest temperature and all the data provided by the embedded sensors translated this difference. The stiffness analysis did not allow to draw conclusions due to the small number of specimens, but the fact that some specimens with embedded sensor showed no significant changes in stiffness, compared with specimens without sensors and surface sensors, reinforces the need to continue with studies in this area that allow to generalize the results.

References

[1] F. P. Beer, E. R. J. Jr, J. DeWolf, and D. F. Mazurek. *Mecânica dos Materiais*. AMGH Editora, Porto Alegre: Brasil, 7 edition, 2015. ISBN: 978-8580554991.

[2] W. Broughton, L. Crocker, and M. Gower. Design requirements for bonded and bolted composite structures. Technical Report NPL Report MATC(A)65, National Physical Laboratory, Teddington, UK, January 2002. ISSN: 1473 2734.

[3] O. Castro, J. M. Silva, T. Devezas, A. Silva, and L. Gil. Cork agglomerates as an ideal core material in lightweight structures. *Materials & Design*, 31(1):1425432, January 2010. doi: 10.1016/j.matdes.2009.05.039.

[4] K. Hoffmann. *Applying the wheatstone bridge circuit*. Hottinger Baldwin Messtechnik GmbH, Darmstadt, Darmstadt, Germany, January 1986.

[5] K. Hoffmann. *An introduction to measurements using strain gages*. Hottinger Baldwin Messtechnik GmbH, Darmstadt, December 1989.

[6] Z.-M. Huang and Y.-X. Zhou. *Strength of fibrous composites*. Advanced Topics in Science and Technology in China. Zhejiang University Press AND Springer, Hangzhou, RPC and Berlin/Heidelberg, Germany, January 2012. ISBN: 978-3642229572/ 978-7308082686 doi: 10.1007/978-3642229589.

[7] G. C. Kahandawa, J. Epaarachchi, H. Wang, and K. Lau. Use of FBG sensors for SHM in aerospace structures. *Photonic Sensors*, 2(3):203214, September 2012. doi: 10.1007/s13320-012-0065-4.

[8] K.-S. Kim, M. Breslauer, and G. S. Springer. The effect of embedded sensors on the strength of composite laminates. *Journal of Reinforced Plastics and Composites*, 11(8):949958, August 1992. doi: 10.1177/073168449201100806.

[9] Z. Li and M. J. Crocker. A review of vibration damping in sandwich composite structures. *International Journal of Acoustics and Vibration*, 10(4):159169, December 2005. doi: 10.20855/ijav.2005.10.4184.

[10] F. Mujika, N. Carbajal, A. Arrese, and I. Mondragon. Determination of tensile and compressive moduli by flexural tests. *Polymer testing*, 25(6):766–771, September 2006. doi:10.1016/j.polymertesting.2006.05.003.

[11] A. Panopoulou, T. Loutas, D. Roulias, S. Fransen, and V. Kostopoulos. Dynamic fiber bragg gratings based health monitoring system of composite aerospace structures. *Acta Astronautica*, 69(7-8):445457, September 2011. doi:10.1016/j.actaastro.2011.05.027.

[12] M. Ramos. Produção e caracterização de materiais compósitos à base de aglomerado de cortiça. Master's thesis, Instituto Superior Técnico, Novembro 2018.

[13] G. Sala, M. Olivier, P. Bettini, and D. Sciacovelli. Embedded piezoelectric sensors and actuators for control of active composite structures. Dipartimento di Ingegneria Aerospaziale, Politecnico di Milano, Mechanical and Thermal Engineering Department, Carlo Gavazzi Space ESTEC, European Space Agency, 2004.

[14] M. Sutton, W. Wolters, W. Peters, W. Ranson, and S. McNeill. Determination of displacements using an improved digital correlation method. *Image and vision computing*, 1(3):133139, August 1983. doi:10.1016/0262-8856(83)90064-1.

[15] N. Takeda, N. S. Minakuchi, and Y. Okabe. Smart composite sandwich structures for future aerospace application-damage detection and suppression-: A review. *Journal of Solid Mechanics and Materials Engineering*, 1(1):3–17, January 2007. doi: 10.1299/jmmp.1.3.

[16] Y. Zhou, C. Sun, Y. Song, and J. Chen. Image pre-filtering for measurement error reduction in digital image correlation. *Optics and Lasers in Engineering*, 65:4656, February 2015. doi: 10.1016/j.optlaseng.2014.04.018.

<table>
<tr><th colspan="3">BATCH TD</th><th colspan="2">BATCH TE</th></tr>
<tr><td colspan="3">Specimens without sensors</td><td colspan="2">Specimens without sensors</td></tr>
<tr><td>TD1</td><td>TD2</td><td>TD3</td><td>TE1</td><td>TE2</td></tr>
<tr><td colspan="3"> 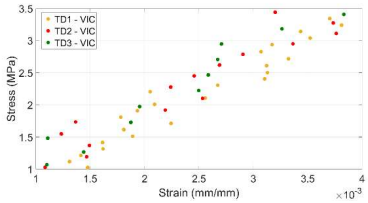

$E_{TD1} = 853{,}8\ MPa$
$E_{TD2} = 833{,}8\ MPa$
$E_{TD3} = 881{,}9\ MPa$</td><td colspan="2"> 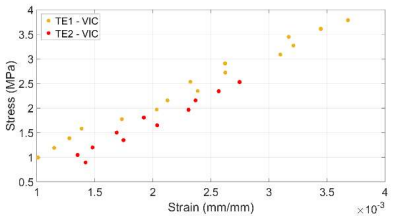

$E_{TE1} = 1034{,}9\ MPa$
$E_{TE2} = 1098{,}1\ MPa$</td></tr>
<tr><td colspan="3">Specimen with surface sensor</td><td colspan="2">Specimen with surface sensor</td></tr>
<tr><td colspan="3">TD/SG1/S</td><td colspan="2">TE/SG1/S</td></tr>
<tr><td colspan="3"> 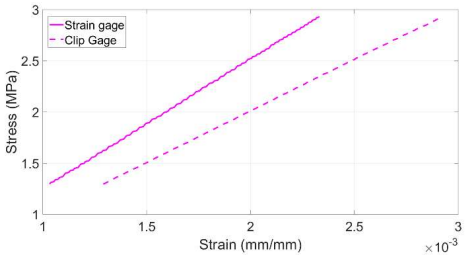

$E_{SG} = 1263{,}8\ MPa$
$E_{CLIP\ GAGE} = 1003{,}3\ MPa$</td><td colspan="2"> 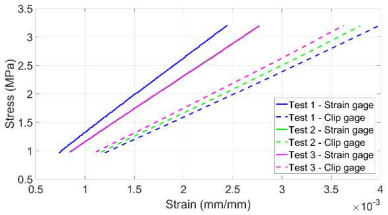

$Test\ 1: E_{SG} = 1185{,}5\ MPa$
$E_{CLIP\ GAGE} = 801{,}9\ MPa$
$Test\ 2: E_{SG} = 1152{,}0\ MPa$
$E_{CLIP\ GAGE} = 839{,}3\ MPa$
$Test\ 3: E_{SG} = 1149{,}5\ MPa$
$E_{CLIPGAGE} = 881{,}6\ MPa$</td></tr>
<tr><td colspan="3">Specimen with embedded sensor</td><td colspan="2">Specimen with embedded sensor</td></tr>
<tr><td>TD/SG1/E</td><td colspan="2">TD/FBG1/E</td><td colspan="2">TE/SG1/E</td></tr>
<tr><td> 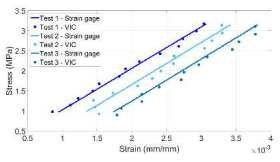

$Test\ 1: E_{SG} = 1035{,}3\ MPa$
$E_{VIC} = 1027{,}2\ MPa$
$Test\ 2: E_{SG} = 1045{,}2\ MPa$
$E_{VIC} = 1022{,}4\ MPa$
$Test\ 3: E_{SG} = 1048{,}5\ MPa$
$E_{VIC} = 1017{,}2\ MPa$</td><td colspan="2"> 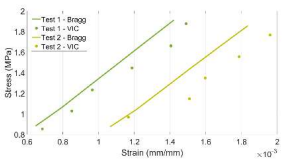

$Test\ 1: E_{BRAGG} = 1337{,}6\ MPa$
$E_{VIC} = 1208{,}1\ MPa$
$Test\ 2: E_{BRAGG} = 1284{,}9\ MPa$
$E_{VIC} = 1033{,}8\ MPa$</td><td> 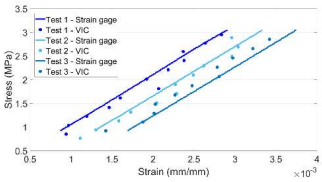

$Test\ 1: E_{SG} = 1056{,}8\ MPa$
$E_{VIC} = 1070{,}7\ MPa$
$Test\ 2: E_{SG} = 1039{,}1\ MPa$
$E_{VIC} = 1048{,}5\ MPa$
$Test\ 3: E_{SG} = 1034{,}4\ MPa$
$E_{VIC} = 1028{,}7\ MPa$</td></tr>
</table>

Figure 3: Results of tensile tests.